Vehicle System Dynamics
2004, Vol. 41, No. 4, pp. 301–322

Taylor & Francis
Taylor & Francis Group

A New Wheel/Rail Spatially Dynamic Coupling Model and its Verification

G. CHEN[1] AND W.M. ZHAI[2]

SUMMARY

Based on the theory of vehicle-track coupling dynamics, a new wheel/rail spatially dynamic coupling model is established in this paper. In consideration of rail lateral, vertical and torsion vibrations and track irregularities, the wheel/rail contact geometry, the wheel/rail normal contact force and the wheel/rail tangential creep force are solved in detail. In the new wheel/rail model, the assumption that wheel contacts rail rigidly and wheel always contacts rail is eliminated. Finally, by numeric simulation comparison with international well-known software NUCARS, comparison with vehicle-track vertical coupling model, and comparison with running test results by China Academy of Railway Sciences, the new wheel/rail spatially dynamic coupling model is shown to be correct and effective.

1. INTRODUCTION

Wheel/rail spatially dynamic coupling model is the basis of the vehicle-track coupling dynamics [1, 2]. By comparison with traditional vehicle dynamics, the vehicle-track coupling dynamics fully considers track vibration and the influence of track irregularities on wheel/rail contact relationship and wheel/rail forces. Therefore, the wheel/rail relationship should be very different between vehicle-track coupling dynamics model and traditional vehicle dynamics model, generally, the rigid contact assumption and the assumption of continuous contact of wheel/rail are made in the solution of the traditional vehicle dynamics model. Kik et al. [3] have considered the elasticity of wheels and rails and given simultaneous treatment of wheel/rail contact force and geometry evaluation when modeling the quasi-static curing behavior. In this paper, a new wheel/rail spatially dynamic coupling model is put forward, which includes wheel/rail dynamically contact model, wheel/rail normal force model, and wheel/rail creep force model. The new wheel/rail model is suitable to full dynamics

[1]Address correspondence to: G. Chen, Civil Aviation College, Nanjing University of Aeronautics and Astronautics, Nanjing, 210016, P.R. China. E-mail: cgzyx@263.net
[2]Train & Track Research Institute, Southwest Jiaotong University, Chengdu, 610031, P.R. China. E-mail: wmzhai@home.swjtu.edu.cn

10.1080/00423110412331315178$22.00

problems including dynamic curving problems and will provide the basis for vehicle-track coupling dynamics analysis.

2. WHEEL/RAIL COORDINATE SYSTEMS

Because wheel/rail coordinate systems are the basis for wheel/rail relationship, they must be defined first. Figure 1 shows the definitions of wheelset and rail coordinates, the rotation transform relationships between coordinates are ignored here due to limited space. Each coordinate is described in detail as follows:

(1) *O-XYZ*: Absolute coordinate. It fixes at the center of wheelset mass, when wheel just contacts and does not compress rail. It does not change with wheel moving. Its vector basis is $\vec{e} = [\vec{i}, \vec{j}, \vec{k}]$.

(2) O_1-$X_1Y_1Z_1$: It fixes at the center of wheelset mass, and shows wheelset parallel move $X(t)$, $Y(t)$, and $Z(t)$ along X, Y, and Z directions, its vector basis is $\vec{e}_1 = [\vec{i}_1, \vec{j}_1, \vec{k}_1]$, and $\vec{e}_1 = \vec{e}$.

(3) O_2-$X_2Y_2Z_2$: It fixes at the center of wheelset mass, and is one of the coordinates, which change with wheelset moving. It shows the yaw move ψ(t) of wheelset to rail, its vector basis is $\vec{e}_2 = [\vec{i}_2, \vec{j}_2, \vec{k}_2]$.

(4) O_3-$X_3Y_3Z_3$: It fixes at the center of wheelset mass, and is one of the coordinates, which change with wheelset moving. It shows the rolling move ϕ(t) of wheelset to rail, its vector basis is $\vec{e}_3 = [\vec{i}_3, \vec{j}_3, \vec{k}_3]$.

(5) C_L-$e_{1L}e_{2L}e_{3L}$: It fixes at left contact spot of wheel/rail, and changes with wheelset moving, its vector basis is $\vec{e}_L = [\vec{i}_{1L}, \vec{j}_{2L}, \vec{k}_{3L}]$.

(6) C_R-$e_{1R}e_{2R}e_{3R}$: It fixes at right contact spot of wheel/rail, and changes with wheelset moving, its vector basis is $\vec{e}_R = [\vec{i}_{1R}, \vec{j}_{2R}, \vec{k}_{3R}]$.

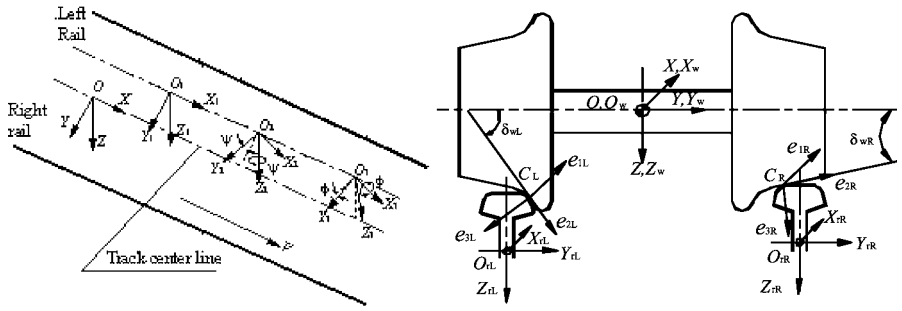

Fig. 1. Definitions of wheelset and rail coordinates.

(7) O_{rL}-$X_{rL}Y_{rL}Z_{rL}$: It fixes at the center of left rail mass, and changes with left rail moving. It shows left rail lateral and vertical parallel move, and rotation around center of its mass, its vector basis is $\vec{e}_{rL} = [\vec{i}_{rL}, \vec{j}_{rL}, \vec{k}_{rL}]$.
(8) O_{rR}-$X_{rR}Y_{rR}Z_{rR}$: It fixes at the center of right rail mass, and changes with right rail moving. It shows right rail lateral and vertical parallel move, and rotation around center of its mass, its vector basis is $\vec{e}_{rR} = [\vec{i}_{rR}, \vec{j}_{rR}, \vec{k}_{rR}]$.

3. WHEEL/RAIL SPATIALLY DYNAMIC COUPLING MODEL

3.1. Wheel/Rail Contact Geometry Relationship Model

Trace curve method [4] is the common computation method of wheel/rail spatial contact geometry. According to trace curve method wheel/rail spatial contact points are only on a curve, which is named trace curve, and wheel whole tyre and rail surface can be replaced by a trace curve. Therefore, 2D scanning can be replaced by 1D scanning through trace curve.

Traditional wheel/rail contact geometry computation method, has two hypotheses [4]: (1) wheel and rail are all regarded as rigid body, and their elastic deformation is not considered; (2) wheel contacts rail all along, and it is not allowed that wheel jumps away from rail. Therefore, traditional wheel/rail contact geometry computation method is: firstly, rail is parallel moved downwards a given distance vertically, then wheelset rolling angle ϕ is adjusted iteratively until left and right minimum vertical distances between wheel and rail surfaces are equal, and finally, wheel/rail contact point coordinate and other parameters, corresponding given lateral displacement y_w and yaw angle ψ, are acquired [4].

In fact, wheel and rail are all elastic, and wheel can sometimes jump away from rail too. Obviously, the two hypotheses of traditional wheel/rail contact geometry relationship do not accord with the reality. For this reason, a new wheel/rail contact geometry relationship solution model is put forward in this paper. The new model can thoroughly abandon two hypotheses that wheel and rail are rigid, and wheel contacts rail all along.

The basic idea or concept of new wheel/rail contact geometry model is: when wheel contacts rail, left wheel/rail minimum vertical distance is not equal to the right, the difference reflects just the difference of the left and right wheel/rail normal compressing amount, and then reflects the difference of left and right wheel/rail normal force and wheel/rail creep force. Obviously, by comparison with traditional solution method, the iteration process of wheelset rolling angle can be avoided. Its detail solution process is: at t moment, the lateral displacement y_w and the yaw angle ψ of wheelset, the lateral displacement y_r, vertical displacement z_r and the torsion angle ϕ_r of rail, and the track irregularities are all known. After wheelset rolling angle

ϕ at t moment, which is solved from equations, is input into wheel/rail contact program, only through computing one time, left and right wheel/rail minimum vertical distance ΔZ_{wjLt} and ΔZ_{wjRt} are obtained, and then left and right wheel/rail contact points coordinates and corresponding parameters are acquired.

Thus it can be seen that the new wheel/rail contact geometry model, avoids iteration solution of wheelset rolling angle, fully considers wheel/rail elastic deformation and instantaneous separation, and breaks through two hypotheses of traditional wheel/rail contact solution. Obviously, it is more reasonable than traditional solution.

3.2. Wheel/Rail Normal Force Computation Model

According to Hertz non-linear contact theory [1], Wheel/rail normal force,

$$N(t) = \left[\frac{1}{G}\delta Z_N(t)\right]^{3/2} \tag{1}$$

Where G is the wheel/rail contact constant (m/N$^{2/3}$); and $\delta Z_N(t)$ is the normal compressing amount at wheel/rail contact point (m).

If wheel is coned tyre (TB), $G = 3.86R^{-0.115} \times 10^{-8}$ (m/N$^{2/3}$); if wheel is worn tyre (LM), $G = 4.57R^{-0.149} \times 10^{-8}$ (m/N$^{2/3}$). Here, R is the wheel nominal radius (m).

Therefore, in order to solve wheel/rail normal force correctly, the key is to obtain normal compressing amount of every moment at wheel/rail contact point. When only wheel/rail vertical vibration is considered, wheel/rail normal compressing amount is vertical relative displacement of wheel and rail [1], and it is very simple. But when wheel/rail lateral and vertical vibrations are considered at the same time, the factors impacting on wheel/rail normal compressing amount are a lot, such as wheelset lateral displacement, wheelset vertical displacement, wheelset yaw angle, wheelset rolling angle, rail lateral displacement, rail vertical displacement, rail torsional angle and track irregularities. Therefore it is very difficult to solve wheel/rail normal compressing amount at every moment after comprehensively considering all factors [2].

From the above analysis, in order to acquire wheel/rail compressing amount at wheel/rail contact point briefly, the key is to avoid the complex method, which considers every influence factor of wheelset and rail at the same time. The new method solving wheel/rail normal compressing amount briefly is introduced as follows.

In fact, wheel/rail lateral relative displacement can be transformed into vertical displacement. Its principle is showed in Figure 2. ΔY is the lateral displacement that wheel compresses rail from C_1 to C, and ΔZ is the vertical displacement that wheel compresses rail from C_2 to C. Obviously, the projections on normal direction of ΔY and ΔZ are both Δn. Therefore wheel/rail normal compressing amount can be acquired simply through transforming ΔY into ΔZ. By combining with contact geometry relationship computation the equivalent model of lateral and vertical displacement simplifies the computation of wheel/rail normal force, and its principle is as follows.

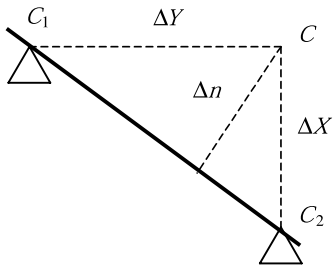

Fig. 2. The lateral and vertical distance of contact plans prior and after compression.

In wheel/rail contact geometry relationship model, when at t moment, the lateral displacement, the yaw angle and the rolling angle of wheelset, the lateral displacement, the vertical displacement and the torsion angle of rail, and the track irregularities are all known, left and right wheel/rail minimum vertical distance ΔZ_{wjLt} and ΔZ_{wjRt} can be obtained through wheel/rail contact computation program. Their values are just synthetic results of all factors, therefore, wheel/rail lateral and vertical relative displacements are transformed into vertical displacements. To obtain left and right wheel/rail vertical relative displacement at t moment, left and right minimum vertical distance of the j_{th} wheelset ($j = 1, 2, 3, 4$) at zero moment ΔZ_{wjL0} and ΔZ_{wjR0} (due to symmetry relationship, $\Delta Z_{wjL0} = \Delta Z_{wjR0} = \Delta Z_{wj0}$) should be subtracted. If wheelset moves ΔZ_{wj0} downwards, wheelset just contacts and does not compress rails. Therefore, left and right wheel/rail vertical relative displacement is,

$$\begin{cases} \delta Z_{Lj} = Z_{wj}(t) - (\Delta Z_{wjLt} - \Delta Z_{wj0}) \\ \delta Z_{Rj} = Z_{wj}(t) - (\Delta Z_{wjRt} - \Delta Z_{wj0}) \end{cases} \quad (j = 1, 2, 3, 4) \tag{2}$$

Where, $Z_{wj}(t)$ is the vertical displacement of j_{th} wheelset at t moment (it is not considered in contact program).

Obviously, when δZ_{Lj} or (and) δZ_{Rj} is (are) less than 0, wheel jumps away from rail, and wheel/rail normal force is zero. Common wheel/rail contact conditions are shown in Figure 3. In Figure 3, (a) shows that left wheel contacts left rail, and right

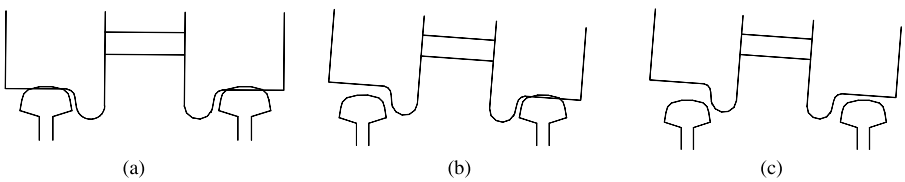

Fig. 3. Wheel/rail contact conditions.

wheel contacts right rail at the same time; (b) shows that left wheel separates from left rail, and right wheel contacts right rail, so it represents one side wheel separates from rail, and the other side wheel contacts rail; (c) shows that left wheel separates from left rail, and right wheel separates from rail too. Obviously, (a) is normal wheel/rail contact state, and belongs to most common wheel/rail contact condition, but (b) and (c) can appear sometimes in practice, particularly, the probability of (b) is more. For the above analysis, the method in this paper can solve the wheel/rail normal force under every wheel/rail contact condition. Because traditional method cannot solve the condition that wheel instantaneously jumps away from rail, the method in this paper is an important development. In order to obtain normal compressing amount, the vertical relative displacement need to be projected on normal direction, that is,

$$\delta_{3L} = \cos(\delta_L + \phi) \cdot \delta Z_{Lj} \tag{3}$$

$$\delta_{3R} = \cos(\delta_R - \phi) \cdot \delta Z_{Rj} \tag{4}$$

δ_{3L} and δ_{3R}, which are obtained, are left and right wheel/rail normal compressing amount. If substituting them into Equation (1), left and right wheel/rail normal forces can be acquired. The method avoids iteration solution process of traditional vehicle dynamics, and then computation speed is improved greatly.

3.3. Wheel/Rail Creep Force Computation Model

3.3.1. Wheel/Rail Creepage [5]

In wheel/rail contact spot coordinate C-$e_1e_2e_3$, the definitions of longitudinal, lateral, and spin creepage are

$$\xi_x = \frac{V_{w1} - V_{r1}}{V} \qquad \xi_y = \frac{V_{w2} - V_{r2}}{V} \qquad \xi_{sp} = \frac{\Omega_{w3} - \Omega_{r3}}{V} \tag{5}$$

Where, V is wheelset speed on rail, V_{w1}, V_{w2} and Ω_{w1} are the speed of contact ellipse on wheel along Ce_1 axis, Ce_2 axis and around Ce_3 axis, respectively. V_{r1}, V_{r2} and Ω_{r1} are the speed of contact ellipse on rail along Ce_1 axis, Ce_2 axle, and around Ce_3 axis, respectively. Wheel/rail creepages are deduced as follows. In the deducting process, right wheel and right rail are acted as examples.

3.3.1.1. Longitudinal and Lateral Creepage Solution. The parallel move speed of center of wheelset mass in fixed coordinate is $\vec{V}_{ow} = \dot{X}_{ow}\vec{i} + \dot{Y}_{ow}\vec{j} + \dot{Z}_{ow}\vec{k}$; the absolute angle speed of wheelset in fixed coordinate is $\vec{\omega}_w = \dot{\phi}\vec{i}_2 + (-\Omega + \dot{\beta})\vec{j}_3 + \dot{\psi}\vec{k}_1$.

Through coordinate transformation, it can be transformed into fixed coordinate, that is,

$$\vec{\omega}_w = \begin{bmatrix} \dot{\phi}\cos\psi - (-\Omega+\dot{\beta})\cos\phi\sin\psi \\ \dot{\phi}\sin\psi + (-\Omega+\dot{\beta})\cos\phi\cos\psi \\ (-\Omega+\dot{\beta})\sin\phi + \dot{\psi} \end{bmatrix}^T \begin{Bmatrix} \vec{i} \\ \vec{j} \\ \vec{k} \end{Bmatrix} \triangleq \begin{bmatrix} \omega_{wx} \\ \omega_{wy} \\ \omega_{wz} \end{bmatrix}^T \begin{Bmatrix} \vec{i} \\ \vec{j} \\ \vec{k} \end{Bmatrix} \tag{6}$$

If the vector from contact point to center of wheel mass is $\vec{R}_R$, then,

$$\vec{R}_R = \begin{bmatrix} R_{xR}' \\ R_{yR}' \\ R_{zR}' \end{bmatrix}^T \begin{Bmatrix} \vec{i}_3 \\ \vec{j}_3 \\ \vec{k}_3 \end{Bmatrix} = \begin{bmatrix} R_{xR}'\cos\psi - R_{yR}'\cos\phi\sin\psi + R_{zR}'\sin\phi\sin\psi \\ R_{xR}'\sin\psi + R_{yR}'\cos\phi\sin\psi - R_{zR}'\sin\phi\cos\psi \\ R_{yR}'\sin\phi + R_{zR}'\cos\phi \end{bmatrix}^T \begin{Bmatrix} \vec{i} \\ \vec{j} \\ \vec{k} \end{Bmatrix}$$
$$\triangleq \begin{bmatrix} R_{xR} \\ R_{yR} \\ R_{zR} \end{bmatrix}^T \begin{Bmatrix} \vec{i} \\ \vec{j} \\ \vec{k} \end{Bmatrix} \tag{7}$$

The relative speed of contact point to center of wheel mass is,

$$\vec{V}_{RR} = \vec{\omega} \times \vec{R}_R = \begin{vmatrix} \vec{i} & \vec{j} & \vec{k} \\ \omega_x & \omega_y & \omega_z \\ R_{xR} & R_{yR} & R_{zR} \end{vmatrix} = \begin{bmatrix} \omega_{wy}R_{zR} - \omega_{wz}R_{yR} \\ \omega_{wz}R_{xR} - \omega_{wx}R_{zR} \\ \omega_{wx}R_{yR} - \omega_{wy}R_{xR} \end{bmatrix}^T \begin{Bmatrix} \vec{i} \\ \vec{j} \\ \vec{k} \end{Bmatrix} \tag{8}$$

According to speed synthesis theorem, the absolute speeds of right wheel and right rail at contact point are, respectively,

$$\vec{V}_{wR} = \begin{bmatrix} \dot{X}_{ow} + \omega_{wy}R_{zR} - \omega_{wz}R_{yR} \\ \dot{Y}_{ow} + \omega_{wz}R_{xR} - \omega_{wx}R_{zR} \\ \dot{Z}_{ow} + \omega_{wx}R_{yR} - \omega_{wy}R_{xR} \end{bmatrix}^T \begin{Bmatrix} \vec{i} \\ \vec{j} \\ \vec{k} \end{Bmatrix}$$

$$\vec{V}_{rR} = \begin{bmatrix} 0 \\ \delta\dot{Y}_{rL} \\ \delta\dot{Z}_{rL} \end{bmatrix} \begin{Bmatrix} \vec{i} \\ \vec{j} \\ \vec{k} \end{Bmatrix} + \begin{bmatrix} 0 \\ \dot{Y}_{rR} \\ \dot{Z}_{rR} \end{bmatrix} \begin{Bmatrix} \vec{i} \\ \vec{j} \\ \vec{k} \end{Bmatrix}$$

Where, $\dot{Y}_{rR}$, $\dot{Z}_{rR}$: Lateral and vertical vibration speeds of right rail; $\delta\dot{Y}_{rR}$, $\delta\dot{Z}_{rR}$: Lateral and vertical speeds of track irregularities on right rail.

So, absolute speed difference of right wheel/rail at contact point is

$$\Delta\vec{V}_R = \begin{bmatrix} \dot{X}_{ow} + \omega_{wy}R_{zR} - \omega_{wz}R_{yR} \\ \dot{Y}_{ow} + \omega_{wz}R_{xR} - \omega_{wx}R_{zR} - \dot{Y}_{rR} - \delta\dot{Y}_{rR} \\ \dot{Z}_{ow} + \omega_{wx}R_{yR} - \omega_{wy}R_{zR} - \dot{Z}_{rR} - \delta\dot{Z}_{rR} \end{bmatrix}^T \begin{Bmatrix} \vec{i} \\ \vec{j} \\ \vec{k} \end{Bmatrix} = \begin{bmatrix} \Delta V_{xR} \\ \Delta V_{yR} \\ \Delta V_{zR} \end{bmatrix}^T \begin{Bmatrix} \vec{i} \\ \vec{j} \\ \vec{k} \end{Bmatrix} \tag{9}$$

Because creepage is defined in contact spot coordinate, the absolute speed difference should be transformed into contact spot coordinate. The rotation transformation between right wheel/rail contact spot coordinate and absolute coordinate is shown in Equation (10), and the relative speed difference in right wheel/rail contact spot coordinate is shown in Equation (11).

$$\begin{Bmatrix} \vec{e}_{1R} \\ \vec{e}_{2R} \\ \vec{e}_{3R} \end{Bmatrix} = \begin{bmatrix} \cos\psi & \sin\psi & 0 \\ -\cos(\delta_R-\phi)\sin\psi & \cos(\delta_R-\phi)\cos\psi & -\sin(\delta_R-\phi) \\ -\sin(\delta_R-\phi)\sin\psi & \sin(\delta_R-\phi)\cos\psi & \cos(\delta_R-\phi) \end{bmatrix} \begin{Bmatrix} \vec{i} \\ \vec{j} \\ \vec{k} \end{Bmatrix} = B_{\delta R} \begin{Bmatrix} \vec{i} \\ \vec{j} \\ \vec{k} \end{Bmatrix} \tag{10}$$

$$\Delta\vec{V}_R = \vec{e}_R {B_{\delta R}}^{-1} \begin{bmatrix} \Delta V_{xR} \\ \Delta V_{yR} \\ \Delta V_{zr} \end{bmatrix} = \vec{e}_R {B_{\delta R}}^{T} \begin{bmatrix} \Delta V_{xR} \\ \Delta V_{yR} \\ \Delta V_{zR} \end{bmatrix} \triangleq \begin{bmatrix} \Delta V_{1R} \\ \Delta V_{2R} \\ \Delta V_{3R} \end{bmatrix}^T \begin{Bmatrix} \vec{e}_{1R} \\ \vec{e}_{2R} \\ \vec{e}_{3R} \end{Bmatrix} \tag{11}$$

Therefore, according to creepage definitions, the longitudinal and lateral creepages at right wheel/rail contact point are respectively,

$$\xi_{xR} = \frac{\Delta V_{1R}}{V} \qquad \xi_{\mathrm{yR}} = \frac{\Delta V_{2R}}{V} \tag{12}$$

Where, V is vehicle moving speed.

3.3.1.2. Spin Creepage Solution Model. The absolute angle speed of right rail is $\vec{\omega}_{rR} = \dot{\phi}_{rR}\vec{i} + 0\vec{j} + 0\vec{k}$. Here, $\dot{\phi}_{rR}$ is rail torsion angle speed.

Wheelset angle speed has already been obtained in Equation (6), therefore, the relative angle speed difference between wheelset and right rail in absolute coordinate is,

$$\Delta\vec{\omega}_R = \vec{\omega}_w - \vec{\omega}_{rR} = \begin{bmatrix} \dot{\phi}\cos\psi - (-\Omega+\dot{\beta})\cos\phi\sin\psi - \dot{\phi}_{rR} \\ \dot{\phi}\sin\psi + (-\Omega+\dot{\beta})\cos\phi\cos\psi \\ (-\Omega+\dot{\beta})\sin\phi + \dot{\psi} \end{bmatrix} \begin{Bmatrix} \vec{i} \\ \vec{j} \\ \vec{k} \end{Bmatrix} = \begin{bmatrix} \Delta\omega_x \\ \Delta\omega_y \\ \Delta\omega_z \end{bmatrix}^T \begin{Bmatrix} \vec{i} \\ \vec{j} \\ \vec{k} \end{Bmatrix} \tag{13}$$

In the same way, if angle speed difference is transformed into contact point coordinate, the part of angle speed difference in $\vec{e}_3$ can be obtained.

$$\begin{aligned}\Delta\omega_{3R} &= \begin{bmatrix} -\sin(\delta_R-\phi)\sin\psi \\ \sin(\delta_R-\phi)\cos\psi \\ \cos(\delta_R-\phi) \end{bmatrix}^T \begin{bmatrix} \omega_x \\ \omega_y \\ \omega_z \end{bmatrix} \\ &= -\omega_{wx}\sin(\delta_R-\phi)\sin\psi + \omega_{wy}\sin(\delta_R-\phi)\cos\psi + \omega_{wz}\cos(\delta_R-\phi) \end{aligned} \quad (14)$$

Therefore, the spin creepage of right wheel/rail contact point is $\xi_{\text{spR}} = \frac{\Delta\omega_{3R}}{V}$. Here, V is vehicle moving speed.

3.3.2. Creep Force Computation

In this paper, wheel/rail creep force is calculated according to Kalker linear creep theory firstly. Because Kalker linear theory is only fit for small creepage, when large creepage appears, creep force presents saturation, and then creep force is non-linear with creepage. For this reason, Shen-Hedrick-Elkins theory is applied to make non-linear modification [6].

4. VERIFICATION OF NEW WHEEL/RAIL SPATIALLY DYNAMIC COUPLING MODEL

Because the new wheel/rail spatially dynamic coupling model, which is put forward in this paper, is very different from traditional wheel/rail model, and the solutions of wheel/rail contact geometry and normal force break through traditional method, the reasonability and reliability of the new wheel/rail model should be verified fully. For this reason, the vehicle-track vertical and lateral model, which is based on the new wheel/rail model, is established. In order to verify the model and its solution which are put forward in this paper, and lay a foundation for the wide application of new wheel/rail spatially dynamic coupling model, verifications are carried out in four aspects: (1) by vehicle dynamic negotiation comparison with international well-known software NUCARS; (2) by wheel/rail response comparison under the excitation of track vertical profile and alignment irregularities with NUCARS; (3) by vertical random vibration response comparison with single vehicle-track vertical coupling model; (4) by comparison with line experiment of China's main type freight train C_{62A}.

4.1. Vehicle Dynamic Negotiation Numerical Simulation Comparison

Here, vehicle-track vertical and lateral coupling model (based on the new wheel/rail coupling model) and NUCARS software (based on traditional wheel/rail model) are applied to compute vehicle dynamic negotiation, respectively, and their computation

results are compared. Vehicle and track parameters are the same, vehicle speed is 90 km/h, curve track condition is: transition curve length is 50 m, circle curve length is 100 m, circle curve radius is 1000 m, superelevation on curve is 80 mm. Simulation results are shown in Figures 4–7.

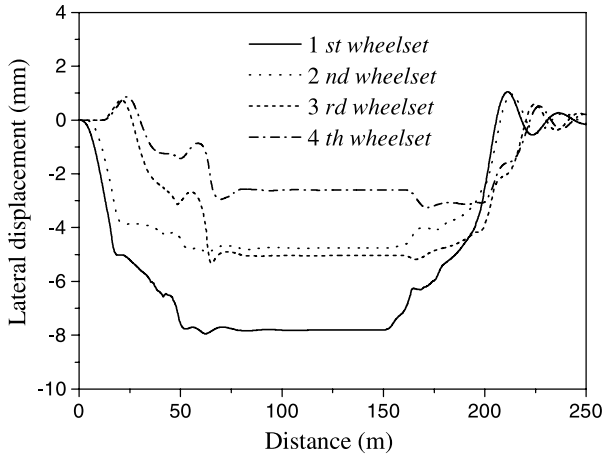

Fig. 4. Wheelset lateral displacement (Coupling model).

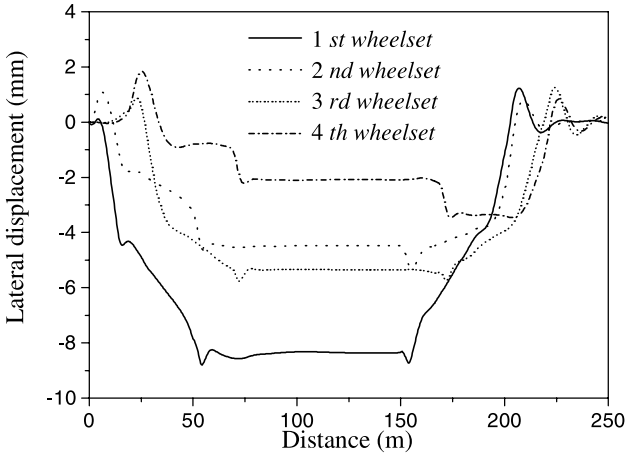

Fig. 5. Wheelset lateral displacement (NUCARS).

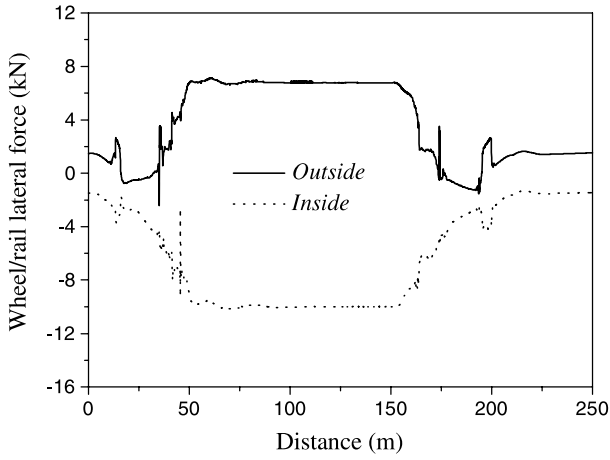

Fig. 6. Wheel/rail lateral force (Coupling model).

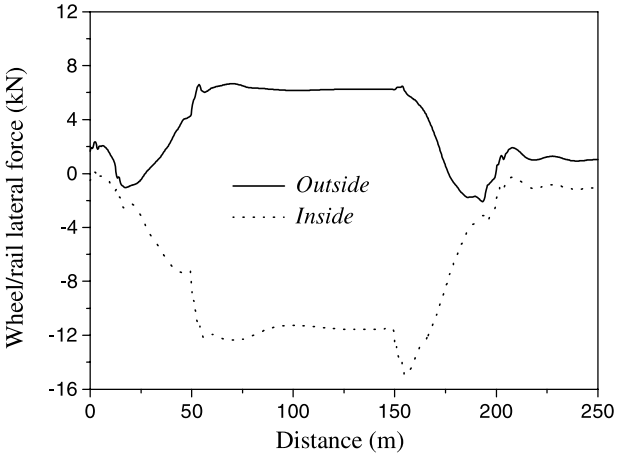

Fig. 7. Wheel/rail lateral force (NUCARS).

From Figures 4 and 5, it can be seen that, for the 1st and the 4th wheelset lateral displacements, the results of NUCARS are 8.2 mm and 2.0 mm, respectively, and the results of vehicle-track vertical and lateral coupling model are 7.8 mm and 2.5 mm, respectively; for 2nd and 3rd wheelset lateral displacement, the results of coupling model are all 5.0 mm, but the results of NUCARS are 4.2 mm and 5.2 mm, respectively.

Because wheel possess LM tyre (worn tyre) which is advantageous to vehicle negotiation, wheel flange usually does not get near rail when vehicle negotiates large radius curve at lower speed. The computation results in this paper just show the law. Directive wheel fringe does not get near rail, therefore, wheel/rail lateral force mainly presents creep force, and the lateral part force of wheel/rail normal force is relatively less. In Figures 6 and 7, the lateral force of directive axle outside wheel is less than inside wheel. Two software both show the trend. Outside and inside wheel lateral forces are respectively: 7 kN and 10 kN (coupling model), 6 kN and 11 kN (NUCARS). Obviously, their results are basically identical. Through comparison of vehicle dynamic negotiation numerical simulation, to some extent, the new wheel/rail coupling model is verified to be reliable and correct.

4.2. Comparison of Numerical Simulation Under the Excitation of Track Vertical Profile and Alignment Irregularities

In order to further verify the new wheel/rail spatially dynamic coupling model, vehicle-track vertical and lateral coupling model (based on the new wheel/rail coupling model) and NUCARS software (based on traditional wheel/rail model) are applied to compute the vibration of vehicle and track systems under the excitation of track vertical profile and alignment irregularities respectively. The vertical profile irregularity mathematic model is indicated in Equation (15); the alignment irregularity mathematic model is indicated in Equation (16). Figures 8–11 are car-body vertical acceleration and wheel/rail vertical force under the excitation of track

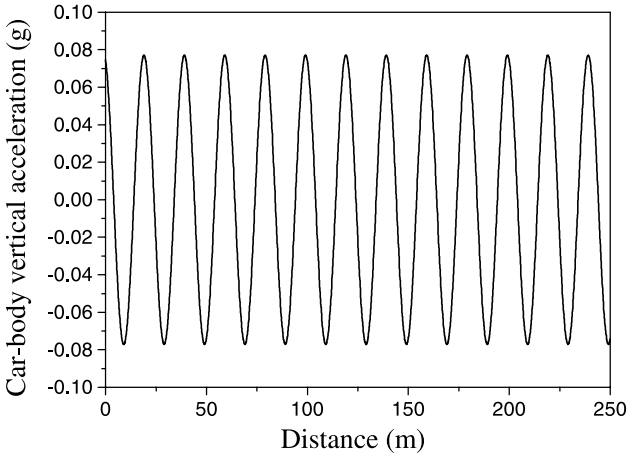

Fig. 8. Car-body vertical acceleration (Coupling model).

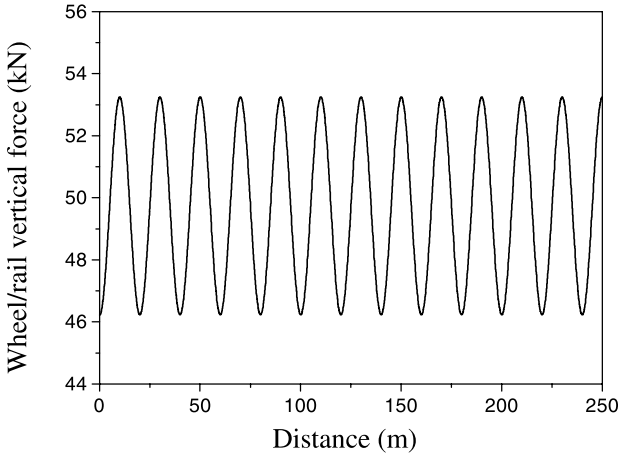

Fig. 9. Wheel/rail vertical force (Coupling model).

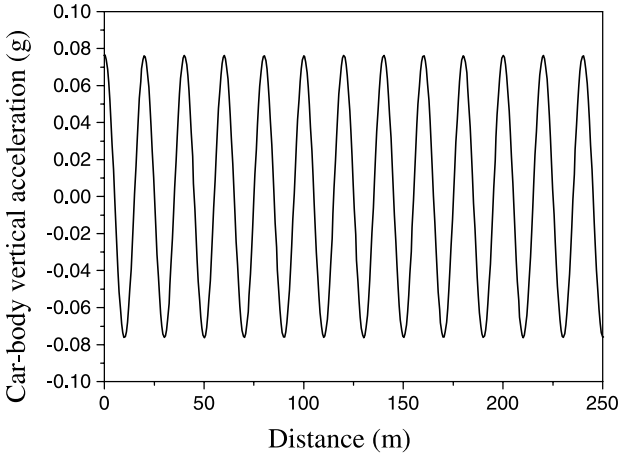

Fig. 10. Car-body vertical acceleration (NUCARS).

vertical profile irregularity; Figures 12–15 are car-body lateral acceleration and wheel/rail lateral force, under the excitation of track alignment irregularity.

Vertical profile irregularity:

$$Z = 0.5A(1 - \cos(2\pi X/\lambda)) \tag{15}$$

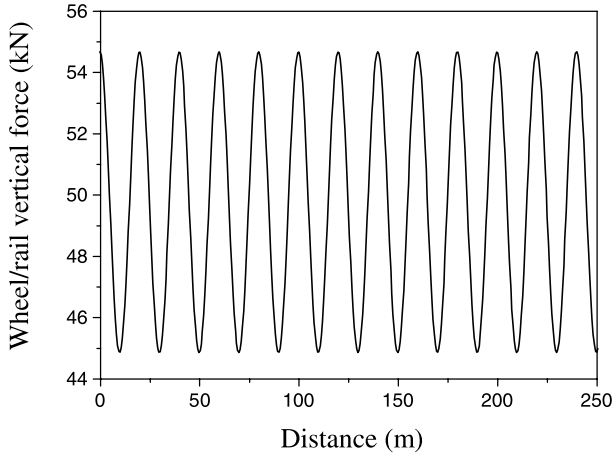

Fig. 11. Wheel/rail vertical force (NUCARS).

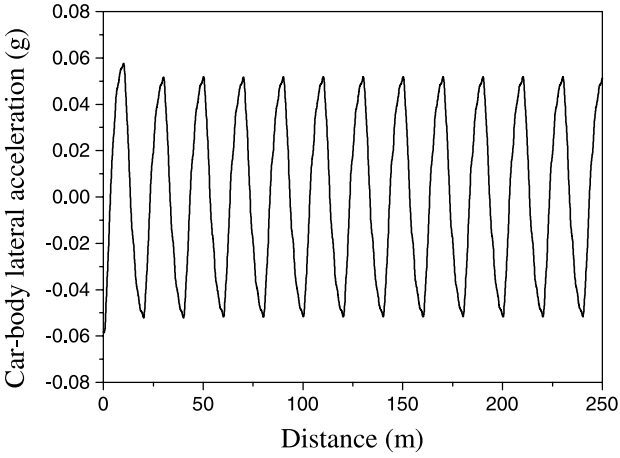

Fig. 12. Car-body lateral acceleration (Coupling model).

Alignment irregularity:

$$Y = 0.5A(1 - \cos(2\pi X/\lambda)) \tag{16}$$

Where, A is irregularity peak-peak value; X is track longitudinal distance; λ is irregularity wavelength. In simulation, $\lambda = 20\,\text{m}$, $A = 10\,\text{mm}$, $V = 160\,\text{km/h}$.

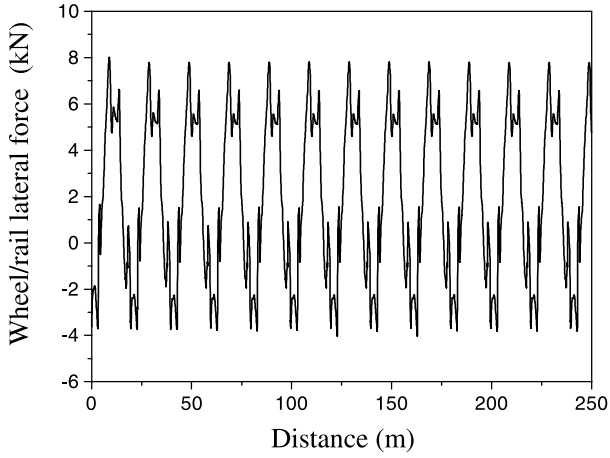

Fig. 13. Wheel/rail lateral force (Coupling model).

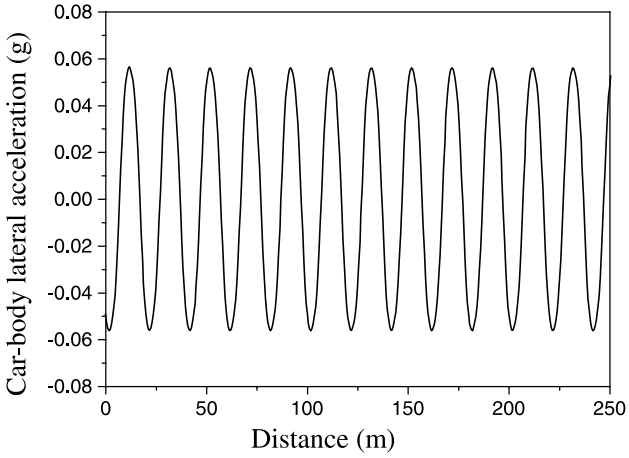

Fig. 14. Car-body lateral acceleration (NUCARS).

Under the excitation of track vertical profile irregularity, comparing Figure 8 with Figure 10, car-body vertical acceleration is 0.077 g (coupling model), and 0.075 g (NUCARS); comparing Figure 9 with Figure 11, wheel/rail vertical force is 53.2 kN (coupling model), and 54.6 kN (NUCARS). Under the excitation of track alignment irregularities, comparing Figure 12 with Figure 14, car-body lateral acceleration is 0.05 g (coupling mode), and 0.057 g (NUCARS); comparing Figure 13 with

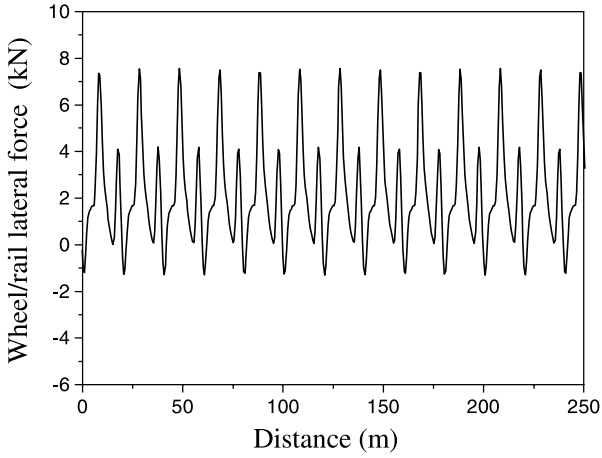

Fig. 15. Wheel/rail lateral force (NUCARS).

Figure 15, wheel/rail lateral force is 8 kN (coupling mode) and 7.5 kN (NUCARS). Therefore, their results are basically identical.

4.3. Comparison of Vertical Random Vibration Responses of Vehicle and Track Systems With Single Vehicle-Track Vertical Coupling Model

Literature [1] establishes the vehicle-track vertical coupling model in detail, which is regarded as a weak non-linear system, in which vehicle and track systems are linear spring-damping systems, and only wheel/rail contact spring is a non-linear component, but it can be linearized. Therefore, vertical random vibration of vehicle-track vertical coupling system can be studied by using mature linear system random vibration theory. At present, in random vibration research domain, frequency domain method is still dominant, which acquires system response PSD through multiplying system frequency response function and track irregularities PSD.

In acquiring vehicle and track vertical random vibration responses, vehicle-track vertical and lateral model adopts numerical integration methods, and considers wheel/rail contact relationship and wheel/rail creep force. However, vehicle-track vertical coupling model adopts frequency domain method, and does not consider wheel/rail contact relationship and wheel/rail creep force. In terms of the calculation of wheel/rail normal force, two models are very different, and vertical and lateral coupling model is much more complex than single vertical coupling model.

The vehicle and track random responses PSD are compared in detail as follows. Track vertical profile irregularity excitation is American 6th grade track spectrum [6],

and vehicle speed is 160 km/h. Because the outputs which are solved by vehicle-track vertical and lateral coupling model, are time series, they should be made PSD estimate in order to acquire PSD. In this paper, PSD estimate method is Blackman-Turkey method [7].

From Figures 16–21, it can be seen that, computation results, which are solved using two models respectively, are almost identical. Car-body and wheelset vertical

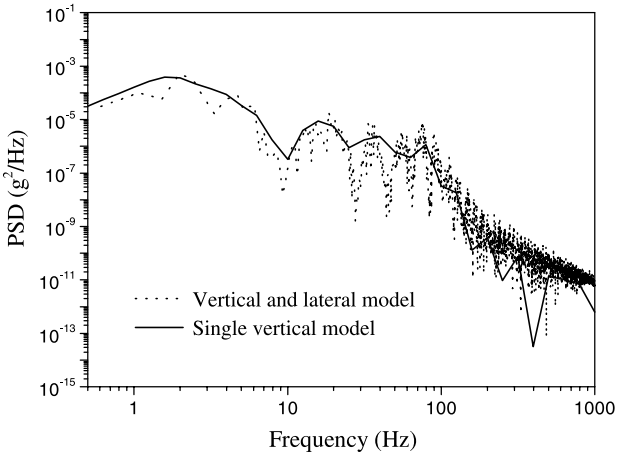

Fig. 16. Car-body vertical acceleration PSD.

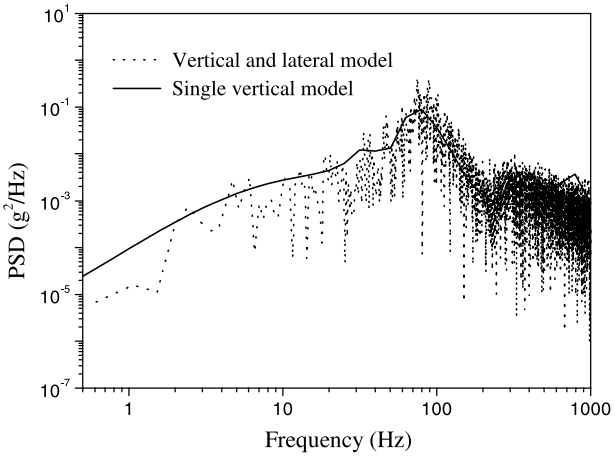

Fig. 17. Wheelset vertical acceleration PSD.

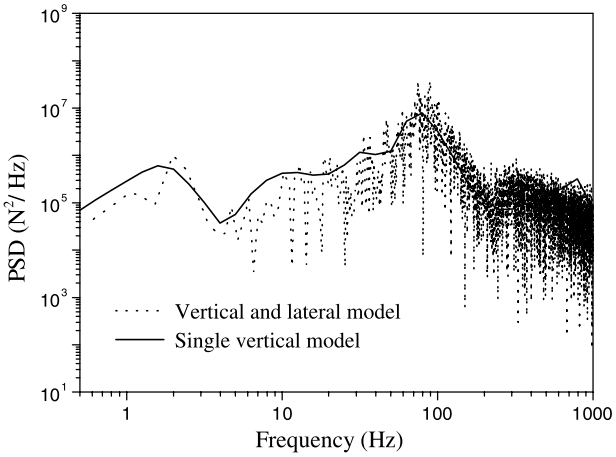

Fig. 18. Wheel/rail vertical force PSD.

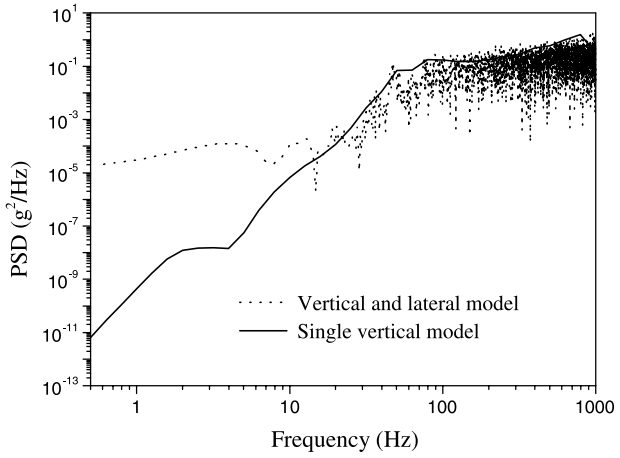

Fig. 19. Rail vertical acceleration PSD.

acceleration PSDs are basically the same in the frequency domain range between 0.5–1000 Hz. Rail, sleeper, and ballast vertical vibration PSDs have some difference in 0.5–10 Hz, but they are basically identical in 10–1000 Hz. Because rail, sleeper main vibration frequencies are tens, hundreds, or thousands, ballast main vibration frequencies are 50–100 Hz too. Obviously, the computation results of two models are very consistent, and the differences in low frequency range under 10 Hz are negligible.

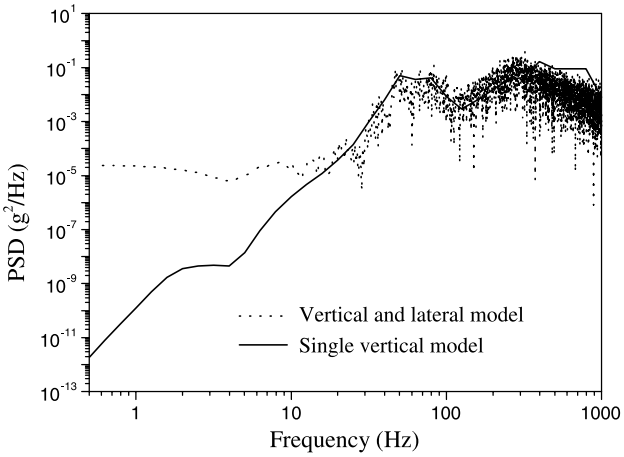

Fig. 20. Sleeper vertical acceleration PSD.

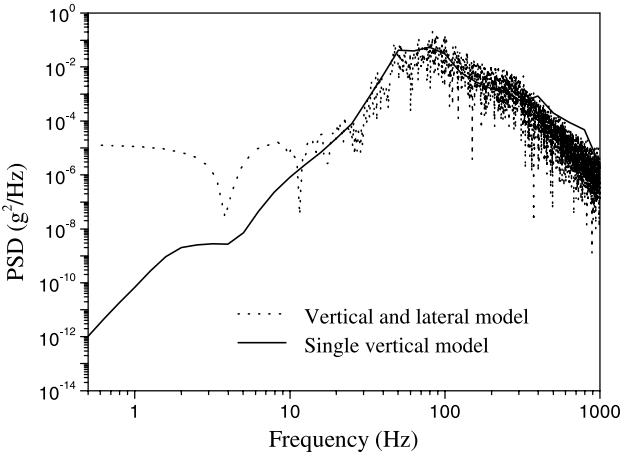

Fig. 21. Ballast vertical acceleration PSD.

4.4. Comparison With Freight Train Derailment Experiment

With train speed increasing and heavy haul railway transportation developing on the existing line, derailment becomes the main factor of influencing transportation safety. In China, since freight train has increased speed in recent years, derailment accidents rise gradually, and this has already seriously affected transportation safety. For this

reason, China Academy of Railway Sciences has made many line experiments in order to evaluate freight train dynamics behaviors. Figure 23 is a experiment result of C62 empty vehicle, and the experiment was done by China Academy of Railway Sciences in December 1999. Vehicle speed is 78 km/h, and track condition is good. From Figure 23, we can see that, because severe hunting move appears, wheel/rail

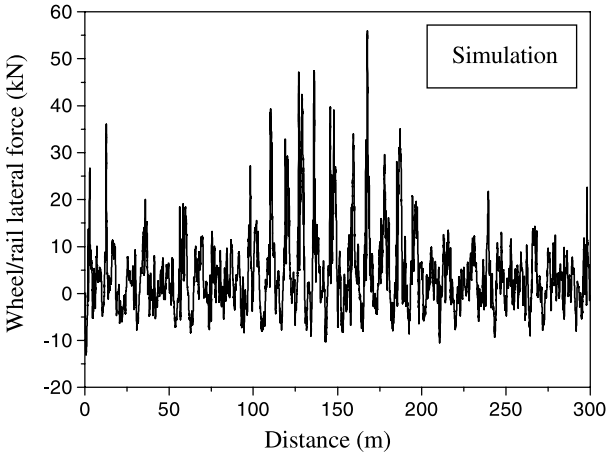

Fig. 22. Wheel/rail lateral force.

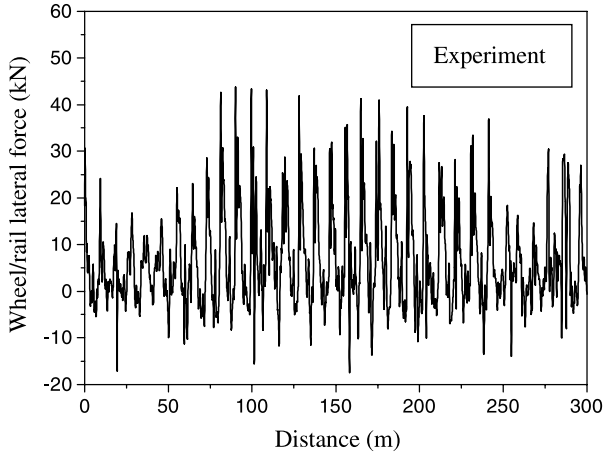

Fig. 23. Wheel/rail lateral force.

lateral force becomes very large, and its maximum reaches 45 kN. Obviously, the probability of vehicle derailment would increase greatly.

Figure 22 is the simulation result, which is obtained by using vehicle-track vertical and lateral model based on new wheel/rail coupling model. Track irregularities are Chinese mainline track spectrum [8]. From Figure 22, it can be seen that simulation result shows severe hunting move of freight vehicle. Comparing Figure 22 with Figure 23, the trend of simulation and experiment result is basically identical.

5. CONCLUSION

In this paper, in consideration of the rail lateral, vertical and torsional vibrations, and the track irregularities, the wheel/rail contact geometry, the wheel/track normal contact force model, and the wheel/rail tangential creep force are solved in detail. The wheel/rail spatially dynamic coupling model is essential for the analysis of the vehicle-track coupling dynamics.

The new wheel/rail model breaks through two hypotheses in traditional wheel/rail model that wheel contacts rail rigidly and wheel contacts rail all along. The iteration solution of wheelset rolling angle is avoided, and wheel/rail contact parameters can be solved quickly. The iteration of wheel/rail normal force and creep force is avoided too, and then the condition that wheel instantaneously jumps away from rail is considered. By Comparison with traditional vehicle dynamics model, the new wheel/rail spatially dynamic coupling model, which is put forward in this paper, is more perfect.

Finally, verifications in four aspects show that the new wheel/rail spatially dynamic coupling model is correct and effective.

ACKNOWLEDGEMENTS

This paper is the main content of the first author's Ph.D. thesis. Here, authors are grateful to associate professor C.B. Cai and professor Q.C. Wang at Train & Track Research Institute of Southwest Jiaotong University, and Professor W.H. Zhang and J. Zeng at National Traction Power Laboratory of Southwest Jiaotong University. In addition National Natural Science Foundation of China under Grant No. 50178061 supported the research work of this paper.

REFERENCES

1. Zhai, W.M.: *Vehicle-Track Coupling Dynamics*, 2nd edition. Chinese Railway Press, Beijing, 2002, pp. 1–78.
2. Zhai, W.M., Cai, C.B. and Guo, S.Z.: Coupling Model of Vertical and Lateral Vehicle/Track Interactions. *Veh. Syst. Dyn.* 26 (1) (1996), pp. 61–69.

3. Kik, W., Knothe, K. and Steinborn, H.: Theory and Numerical Results of a General Quasi-Static Curing Algorithm. The Dynamics of Vehicles on Roads and Tracks. In: *Proceedings of 7th IAVSD Symposium*. Cambridge, August 1983, pp. 414–426.
4. Wang, K.W.: Wheel Contact Point Trace Line and Wheel/Rail Contact Geometry Parameters Computation. *J. Southwest Jiaotong Univ.* 1 (1984), pp. 89–99.
5. Garg, V.K. and Dukkipati, R.V.: *Dynamics of Railway Vehicle Systems*. Academic Press, Canada, 1984, pp. 57–129.
6. Shen, Z.Y., Hedrick, J.K. and Elkins, J.A.: A Comparison of Alternative Creep Force Models for Rail Vehicle Dynamic Analysis. In: *Proceedings of 8th IAVSD Symposium*. MIT, Cambridge, 1983, pp. 591–605.
7. Xu, S.X.: *Random Vibration*. Higher Education Press, Beijing, 1990, pp. 191–230.
8. China Academy of Railway Sciences.: *Research Reports on Chinese Mainline Track Irregularities Power Spectrum*. Beijing, 1999, pp. 1–10.

AUTHOR'S VITAE

Chen G., associate professor of Civil Aviation College, Nanjing University of Aeronautics and Astronautics, Nanjing, P.R. China. He is currently mainly engaged in vehicle dynamics, machine fault diagnosis, image processing, pattern recognition, signal analysis and processing.